American Mineralogist, Volume 72, pages 491–506, 1987

Determining (Al,Si) distribution and strain in alkali feldspars using lattice parameters and diffraction-peak positions: A review

Herbert Kroll
Institut für Mineralogie, Westfälische Wilhelms-Universität, Corrensstrasse 24, D-4400, Münster, West Germany
Paul H. Ribbe
Department of Geological Sciences, Virginia Polytechnic Institute and State University, Blacksburg, Virginia 24061, U.S.A.

Abstract

Al contents (t_i) of the T_i tetrahedral sites have been estimated from $\langle T_i\text{–}O\rangle$ bond lengths of 38 K-rich alkali feldspars. These data were used together with lattice parameters and selected diffraction-peak positions (in degrees 2θ, Cu$K\alpha_1$ radiation) for these feldspars, plus corresponding reference values for low albite, low microcline, analbite, and high sanidine, to obtain new regression equations for estimating structural states (to ±0.02). For monoclinic alkali feldspars,

$$\Sigma t_1 \equiv 2t_1 = \frac{b - 24.8095 + 74.9054c^*}{-3.3261 + 19.5012c^*};\ \Sigma t_1 = \frac{2\theta(060) + 12.1814 - 1.040\,93[2\theta(\bar{2}04)]}{0.6112 + 0.015\,92[2\theta(\bar{2}04)]}.$$

For triclinic alkali feldspars,

$$\Sigma t_1 \equiv (t_1o + t_1m) = \frac{b - 21.5398 + 53.8405c^*}{2.1567 - 15.8583c^*}$$

$$\Sigma t_1 = \frac{2\theta(060) + 8.3063 - 0.964\,59[2\theta(\bar{2}04)]}{-6.5616 + 0.157\,24[2\theta(\bar{2}04)]}.$$

The b-c^* equations produce nearly linear plots for alkali-exchange series, a substantial improvement over the relationships involving b and c cell parameters. The familiar α^*-γ^* plot gives $\Delta t_1 \equiv (t_1o - t_1m)$ for triclinic alkali feldspars; the regression equation is

$$\Delta t_1 = \frac{\gamma^* - 44.778 - 0.502\,46\alpha^*}{6.646 - 0.050\,61\alpha^*}.$$

Equations in terms of $[2\theta(130) - 2\theta(1\bar{3}0)]$ and $2\theta(\bar{2}01)$ are given for Δt_1 in K- and Na-rich feldspars. In addition, other determinative methods for Σt_1 and Δt_1 involving the translations tr[110] and tr[1$\bar{1}$0] are presented.

New quantitative strain indexes (S.I., in %) are defined for phases that occur in coherent or semicoherent perthitic intergrowths: for K-rich feldspars, S.I. = 3391.84 + 67.960a − 42.516($b\cdot c$), and for Na-rich feldspars, S.I. = 1028.00 + 193.883a − 28.472($b\cdot c$). Similar equations were derived using d_{201} and ($d_{060}\cdot d_{204}$).

Introduction

In a study of relations among lattice parameters, composition, and the degree of (Al,Si) order in alkali feldspars, Kroll and Ribbe (1983, p. 67–68) established a method for calculating the average Al content (t_i) of individual tetrahedral sites (T_i) using the results of dozens of modern crystal-structure analyses:

$$t_i = 0.25(1 + n_{An}) + (\langle T_i\text{–}O\rangle - \langle\langle T\text{–}O\rangle\rangle)/\text{const}, \quad (1)$$

where t_i is the Al content or site occupancy of the T_i tetrahedral site (i.e., t_i = number of Al atoms occupying T_i tetrahedra divided by the number of T_i tetrahedra), n_{An} is mole fraction anorthite content, $\langle T_i\text{–}O\rangle$ is the mean of four (Al,Si)–O bond lengths for the T_i tetrahedron, and $\langle\langle T\text{–}O\rangle\rangle$ is the grand mean of all nonequivalent T–O bond lengths in the unit cell (16 of them for triclinic and 8 for monoclinic alkali feldspars). The "const" term is $\langle\langle$Al–O$\rangle\rangle$ − $\langle\langle$Si–O$\rangle\rangle$, and it is equal to 0.125 Å for K-rich and 0.130 Å for Na-rich feldspars. These values represent our assumption that low microcline and low albite are fully ordered, with $t_1o = 1.0$, $t_1m = t_2o = t_2m = 0.0$. In partial confirmation of that assumption, Smith et al. (1986) have refined to $R = 0.005$ the structure of an Amelia, Virginia, low albite at 13 K by neutron diffraction: they found 0.997(4) Al in T_1O and 1.001(3), 1.002(3),

0003–004X/87/0506–0491$02.00

TABLE 1. Al/(Al + Si) in the tetrahedral sites of ordered alkali feldspars, calculated using Equation 1

	Low albite	Low microcline
t_1o	0.996	0.994
t_1m	−0.042	−0.006
t_2o	0.019	0.002
t_2m	0.027	0.010

and 1.006(3) Si in T_1m, T_2O, T_2m, respectively, and $\langle\langle Al–O\rangle\rangle - \langle\langle Si–O\rangle\rangle = 0.1293$ Å.

Although low albite is fully ordered, the three Si tetrahedra are not of equal size: owing to the bonding effects, the T_1m tetrahedron is significantly smaller than the T_2O and T_2m tetrahedra (Phillips and Ribbe, 1973). Consequently, when individual site occupancies are calculated from Equation 1, t_1m values will be too small. This is especially true for Na-feldspars of any state of order, but it is valid to a lesser degree for (low) microcline as well.

TABLE 2. Values of $2t_1$ for metrically monoclinic and $(t_1o + t_1m)$ for topochemically triclinic K-rich alkali feldspars

No.	Sample	⟨T–O⟩	*b*, *c**	*b*, *c*	tr1$\bar{1}$0, *V*	(Σtr, Δtr)$_{cor}$	(060), ($\bar{2}$04)	c_K	Ref.
		a. Metrically monoclinic: Σt_1 (=$2t_1$) × 1000							
1.	W(h)-Eif	538	543	544	549	549	547	577	1
2.	Spencer C(h)	540	545	544	552	553	544	535	1
3.	7002-Eif	604	613	603	616	616	604	598	1
4.	BHPS-Eif	620	613	614	615	615	615	604	1
5.	W-Eif	640	604	624	605	606	624	668	1
6.	OF-Eif	652	614	611	610	611	612	643	1
7.	Spencer C	716	731	727	732	733	729	714	1
8.	Spencer B	828	872	863	877	879	868	852	1
9.	7007	848	859	839	848	849	842	801	1
10.	Himalaya	904	890	895	886	887	899	883	1
11.	SV 1050-Eif	536	540	540	544	544	542	580	3
12.	SV 850-Eif	568	575	571	577	578	572	599	3
13.	SV 0-Eif	620	610	623	610	611	624	677	3
14.	Ge 950-Eif	537	547	542	549	550	544	571	4
15.	Ge 850-Eif	567	583	577	584	585	577	600	4
16.	Ge 750-Eif	596	588	582	588	590	583	609	4
17.	Ge 0-Eif	621	618	616	618	619	617	638	4
18.	Ge-Orma	848	832	828	828	830	830	841	4
19.	P2B†	725	752	756	756	758	753	749	2
20.	P2A†	776	781	791	779	780	791	787	2
21.	CA1A†	842	810	814	802	803	819	823	2
$(\langle\Delta^2\rangle)^{1/2}$			020	017	022	022	017	025	
$\Sigma\{\Delta\}$			006	024	001	−020	−010	−223	
		b. Topochemically triclinic: Σt_1 (=$t_1o + t_1m$) × 1000							
1.	P2B†	725	749	752	775	758	754	749	2
2.	P2A†	776	781	793	795	780	793	787	2
3.	CA1A†	842	814	819	801	803	822	823	2
4.	P17C	813	812	809	814	810	812	801	2
5.	A1D	817	802	799	821	805	803	789	2
6.	CA1B	896	876	888	879	876	886	891	2
7.	P1C	870	898	908	899	896	905	896	2
8.	RC20C	960	965	971	947	960	963	961	2
9.	CA1E	968	980	965	977	982	968	949	2
10.	Spencer U	911	950	930	912	939	923	896	2
11.	Pontiskalk	983	993	976	990	987	981	948	2
12.	Prilep	997	998	995	1002	1001	998	964	2
13.	273	896	867	869	838	853	864	838	3
14.	LCW	862	882	849	861	876	850	836	5
15.	7813A	994	993	994	997	994	996	981	3
16.	7813B	1000	993	994	997	994	996	981	3
17.	PeB	999	994	996	995	994	994	967	6
$(\langle\Delta^2\rangle)^{1/2}$			017‡	017	024	020	016	021	
$\Sigma\{\Delta\}$			001‡	002	009	001	001	252	

Note: Values estimated from mean T–O bond lengths (using Eq. 1 in the text); from *b* and *c** (Eqs. 5 and 6); from *b* and *c* (Eqs. 9 and 10); from tr[1$\bar{1}$0], Δ tr, and *V* (Eqs. 15, 17, and 19); from Σtr_{cor} and Δtr_{cor} (Eq. 24); from $2\theta(060)$ and $2\theta(\bar{2}04)$ (Eqs. 7 and 8); and from c_K (Hovis, 1986, Eqs. 8 and 17; *c* values were taken from his Table 13, except for the nine Adamello intermediate microclines, where the data of DePieri, 1979, were chosen). $(\langle\Delta^2\rangle)^{1/2} = \{1/n[\Sigma(\Sigma t_1\langle T–O\rangle - \Sigma t_1 \text{ (lattice param.)})^2]\}^{1/2}$, where n = number of specimens considered. $\Sigma\{\Delta\} = \Sigma\{\Sigma t_1\langle T–O\rangle - \Sigma t_1 \text{ (lattice param.)}\}$. References: (1) Kroll and Ribbe (1983, Table 2); (2) Kroll and Ribbe (1983, Table 3); (3) Ribbe (1984, Table 4); (4) Gehring (1985); (5) Griffen and Johnson (1984); (6) Blasi et al. (1985).

† Specimen is metrically monoclinic, but topochemically triclinic.

‡ Spencer U was omitted from the regression analysis.

TABLE 3. Values of $\Delta t_1 = (t_1o - t_1m)$ for topochemically triclinic K-rich alkali feldspars (i.e., those with $t_1o > t_1m \geq t_2o = t_2m$)

No.	⟨T–O⟩	α^*, γ^*	Δtr, V	Δtr_{cor}	$\Delta 130$, $\bar{2}01$
	Topochemically triclinic: Δt_1 (=$t_1o - t_1m$) × 1000				
1.†	023	0	0	0	0
2.†	076	0	0	0	0
3.†	102	0	0	0	0
4.	122	105	106	106	107
5.	182	211	215	215	217
6.	419	417	416	417	417
7.	567	521	520	520	525
8.	702	649	645	646	652
9.	914	864	857	857	881
10.	411	376	376	376	366
11.	965	962	957	958	979
12.	994	1011	1006	1008	1005
13.	136	097	096	096	088
14.	224	207	208	208	222
15.	987	1006	1003	1004	1007
16.	1000	1006	1003	1004	1007
17.	997	995	991	992	1000
$(\langle\Delta^2\rangle)^{1/2}$		026	027	027	027

Note: Values estimated from mean T–O bond lengths (Eq. 1; see Table 2 for specimen identification and references), from α^* and γ^* (Eq. 12), from Δtr and V (Eq. 19), from Δtr_{cor} (Eq. 23), and from $\Delta 2\theta(130)$ and $2\theta(\bar{2}01)$ (Eq. 14). $(\langle\Delta^2\rangle)^{1/2}$ as in Table 2, except substitute Σt_1 by Δt_1; $n = 14$.

† Metrically monoclinic specimens not included in n.

TABLE 4. Cell parameters and 2θ values (Cu$K\alpha_1$ radiation, λ = 1.540598 Å) for selected diffraction peaks of alkali feldspar end members

Parameter (units)		Low albite $t_1o = 1.0$	Low microcline $t_1o = 1.0$	Analbite $t_1o = 0.275$	High sanidine $t_1 = 0.275$
a	(Å)	8.135	8.592	8.156	8.605
b	(Å)	12.785	12.963	12.871	13.031
c	(Å)	7.158	7.222	7.108	7.177
c^*	($Å^{-1}$)	0.156552	0.153997	0.157516	0.155023
α	(°)	94.27	90.62	93.52	90.00
α^*	(°)	86.39	90.44	85.94	90.00
β	(°)	116.60	115.95	116.44	116.00
γ	(°)	87.68	87.67	90.26	90.00
γ^*	(°)	90.46	92.29	87.96	90.00
V	($Å^3$)	663.81	722.65	666.44	723.32
tr[110]	(Å)	7.7145	7.9202	7.6031	7.8079
tr[1$\bar{1}$0]	(Å)	7.4366	7.6290	7.6344	7.8079
Δtr	(Å)	0.2779	0.2912	−0.0313	0.0
$\bar{2}01$		22.059	20.992	22.002	20.960
400		50.125	47.049	49.945	46.955
060		42.510	41.813	42.200	41.547
$\bar{2}04$		51.147	50.522	51.486	50.864
130–1$\bar{3}$0		−0.172	−0.815	0.761	0.0
131–1$\bar{3}$1		1.100	−0.807	2.003	0.0

Note: $tr[110] \equiv \frac{1}{2}(a^2 + b^2 + 2ab\cos\gamma)^{1/2}$, $tr[1\bar{1}0] \equiv \frac{1}{2}(a^2 + b^2 - 2ab\cos\gamma)^{1/2}$ $\Delta tr \equiv tr[110] - tr[1\bar{1}0]$.

For example, Equation 1 results in the t values shown in Table 1 for Amelia low albite (Harlow and Brown, 1980; X-ray diffraction data) and Prilep low microcline (Strob, 1983). Negative values for t_1m are physically meaningless, and there cannot be any Al on the T_2 sites, if the T_1O site is fully occupied by Al ($t_1o \approx 1.00$). Thus, we average t_1m, t_2o, and t_2m values for ordered structures (Tables 1 and 3 of Kroll and Ribbe, 1983) and avoid the bias in our determinative method toward disorder. Hovis's (1986) method of estimating site occupancies does not deal with this problem.

Basis for new and revised determinative methods

Equation 1 permits us to estimate average Al contents of the T_1 and T_2 sites of monoclinic and the T_1O, T_1m, T_2O, and T_2m sites of triclinic alkali feldspars whose crystal structures are known. (See references in Table 2 for compositions, direct and reciprocal lattice parameters, mean T–O distances, individual site occupancies, and references for the feldspars used in this study.) These site occupancies are specified for the monoclinic K-rich feldspars as $\Sigma t_1 \equiv 2t_1 = (1 - 2t_2)$ in the ⟨T–O⟩ column of Table 2a and for the triclinic ones as $\Sigma t_1 \equiv (t_1o + t_1m)$ and as $\Delta t_1 \equiv (t_1o - t_1m)$ in the ⟨T–O⟩ columns of Tables 2b and 3, respectively. For triclinic feldspars, individual site occupancies may be calculated as follows: $t_1o = (\Sigma t_1 + \Delta t_1)/2$; $t_1m = (\Sigma t_1 - \Delta t_1)/2$; $t_2o = t_2m = (1 - \Sigma t_1)/2$. These are used in least-squares analyses together with a variety of direct and reciprocal lattice parameters and with calculated 2θ values for hkl peaks in powder patterns to produce a number of new and revised determinative equations and diagrams. The new equations are based on the algorithm of Fletcher and Powell (1963), and the diagrams are now plotted in a manner to mimic the alkali feldspar phase diagram (as suggested by J. V. Smith), i.e., analbite (AA) and/or high albite (HA) and low albite (LA) to the left, high sanidine (HS) and low microcline (LM) to the right, and AA,HA–HS at the top.

In order to preserve a consistent frame of reference for all diagrams, we carefully selected lattice parameters and 2θ angles of certain useful X-ray peaks for these alkali feldspar end members; they are compiled in Table 4. Note that $t_1o = t_1m = 0.275$ is chosen for the AA and HS end members rather than 0.28 as previously assumed. Most values are the same as those in Kroll and Ribbe (1983, Table 2; they have given reasons for the values chosen), but some have been adjusted very slightly.

The familiar b vs. c plot of Wright and Stewart (1968) has been replaced by a pair of b vs. c^* plots and related $2\theta(060)$ vs. $2\theta(\bar{2}04)$ plots (introduced by Wright, 1968), one for monoclinic and one for triclinic alkali feldspars. The purposes are (1) to linearize alkali-exchange paths that on b-c plots are obviously curved and (2) to account for two distinct trends of the b and c^* parameters when plotted against total Al in the T_1 sites for monoclinic and triclinic feldspars (see Fig. 1). Revised α^* vs. γ^* and related $[2\theta(130) - 2\theta(1\bar{3}0)]$ vs. $2\theta(\bar{2}01)$ plots have been calculated for determining $(t_1o - t_1m) \equiv \Delta t_1$, the difference in Al contents of the T_1O and T_1m sites of triclinic feldspars. A complement of (Al,Si) determinative diagrams has been prepared using the translations tr[110] and tr[1$\bar{1}$0] and other parameters. In many of the new diagrams, we have plotted lattice parameters of the two new alkali-exchange series, LA–LM and AA–HS, determined by Kroll et al. (1986). To determine degrees of strain in the K- and Na-rich phases of exsolved alkali feldspars, a

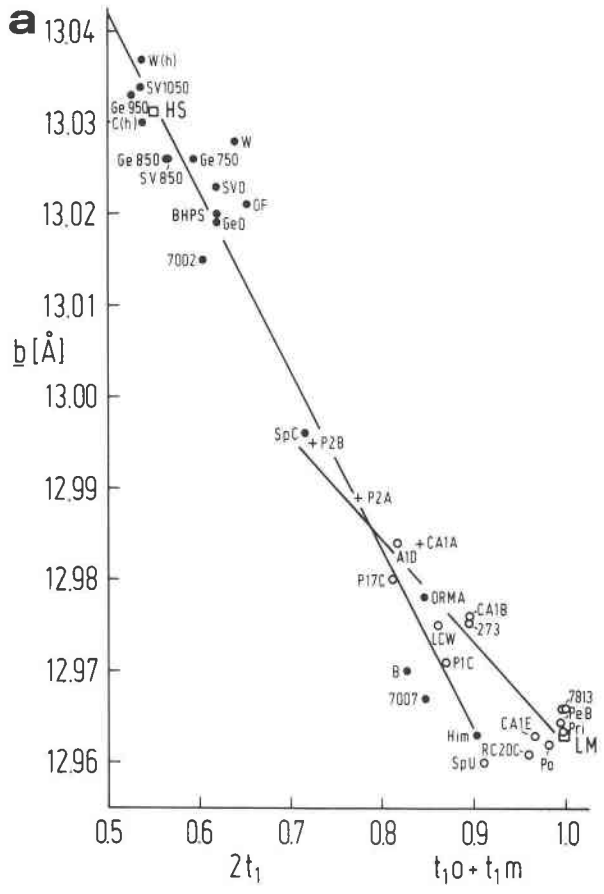
a
b [Å]
13.04
13.03
13.02
13.01
13.00
12.99
12.98
12.97
12.96
W(h)
SV1050
Ge 950
C(h)
HS
W
Ge 850
Ge 750
SV 850
SVO
OF
BHPS
GeO
7002
SpC
+P2B
+P2A
+CA1A
A1O
P17C
ORMA
CA1B
273
LCW
P1C
B
7007
7813
PeB
Pri
LM
Him
CA1E
RC20C
SpU
Po
0.5
0.6
0.7
0.8
0.9
1.0
2t1
t1o + t1m

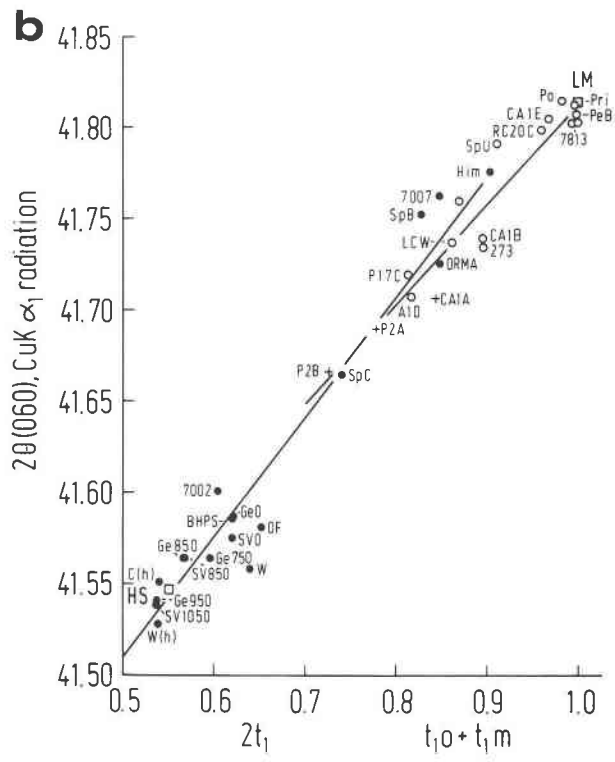
b
2θ(060), CuK α1 radiation
41.85
41.80
41.75
41.70
41.65
41.60
41.55
41.50
LM
Po
Pri
PeB
CA1E
RC20C
7813
SpU
Him
7007
SpB
LCW
CA1B
273
ORMA
P17C
A1O
+CA1A
+P2A
P2B +
SpC
7002
GeO
BHPS
OF
SVO
Ge 850
Ge 750
SV850
W
C(h)
HS
Ge 950
SV1050
W(h)
0.5
0.6
0.7
0.8
0.9
1.0
2t1
t1o + t1m

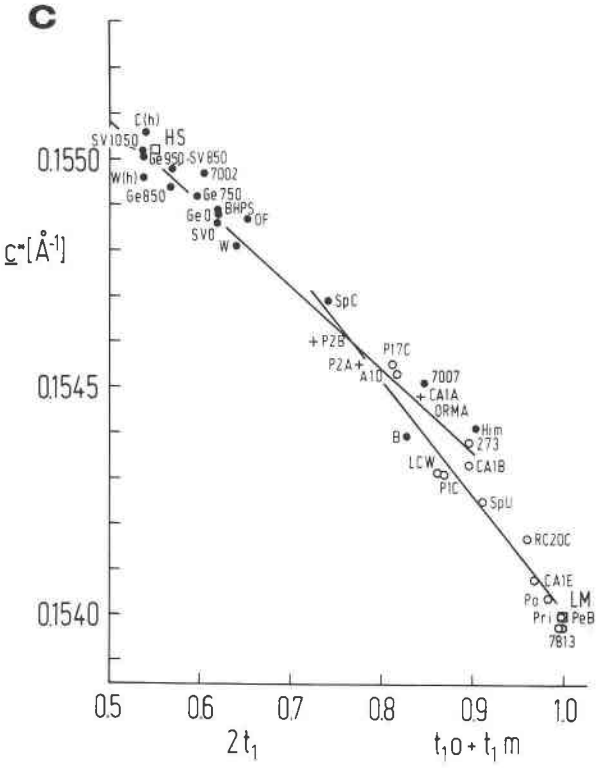
c
c* [Å-1]
0.1550
0.1545
0.1540
C(h)
SV1050
HS
Ge 950
SV 850
7002
W(h)
Ge 850
Ge 750
GeO
BHPS
OF
SVO
W
SpC
+P2B
P2A +
P17C
A1O
7007
+CA1A
ORMA
Him
273
B
LCW
CA1B
P1C
SpU
RC20C
CA1E
Po
LM
Pri
PeB
7813
0.5
0.6
0.7
0.8
0.9
1.0
2t1
t1o + t1m

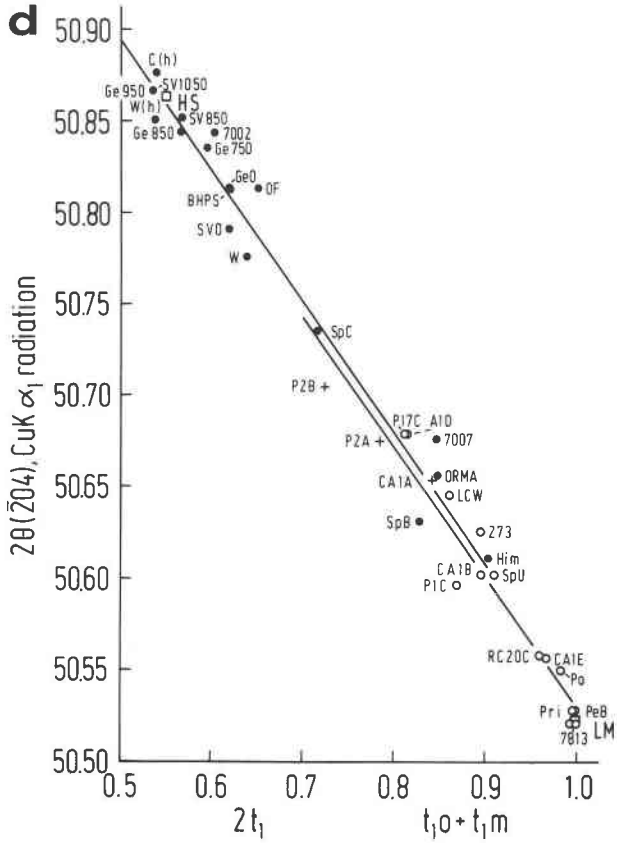
d
2θ(20̄4), CuK α1 radiation
50.90
50.85
50.80
50.75
50.70
50.65
50.60
50.55
50.50
C(h)
Ge 950
SV1050
W(h)
HS
SV 850
Ge 850
7002
Ge 750
GeO
OF
BHPS
SVO
W
SpC
P2B +
P17C
A1O
P2A +
7007
CA1A
ORMA
LCW
SpB
273
Him
CA1B
P1C
SpU
RC20C
CA1E
Po
Pri
PeB
7813
LM
0.5
0.6
0.7
0.8
0.9
1.0
2t1
t1o + t1m

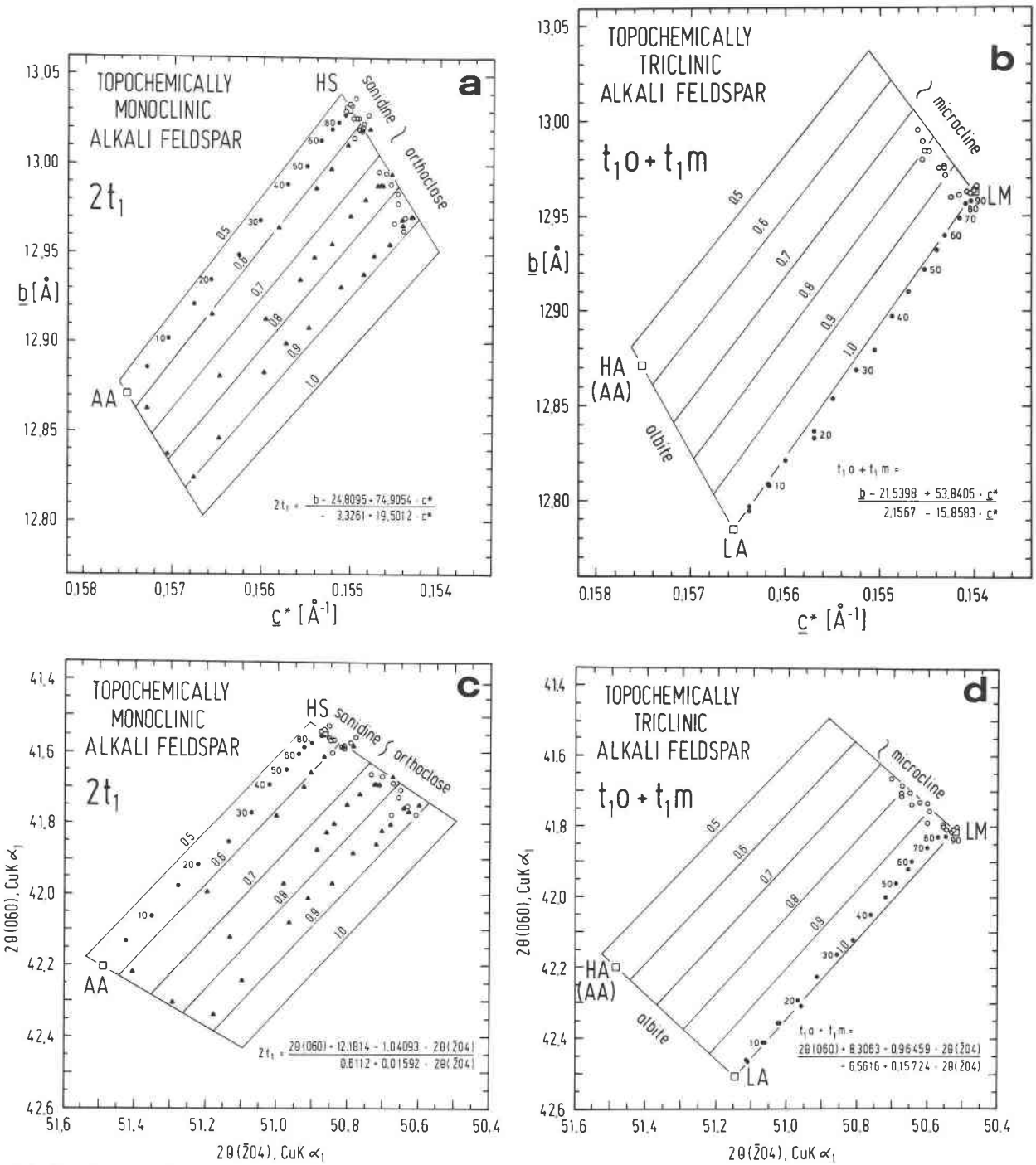

Fig. 2. Diagrams for determining $2t_1$ for "topochemically monoclinic" alkali feldspars, i.e., those with $t_1o = t_1m$ and $t_2o = t_2m$: (a) b vs. c^*, (b) $2\theta(060)$ vs. $2\theta(\bar{2}04)$, and diagrams for determining $(t_1o + t_1m)$ for "topochemically triclinic" alkali feldspars, i.e., those with $t_1o \neq t_1m$: (c) b vs. c^*, (d) $2\theta(060)$ vs. $2\theta(\bar{2}04)$. Circles are data from refined structures (Table 2); dots are data from the LA–LM and AA-HS alkali-exchange series of Kroll et al. (1986); triangles are data from Hovis's (1986) "Eifel sanidine," "orthoclase," and "adularia" exchange series.

←

Fig. 1. Values of $2t_1$ and $(t_1o + t_1m)$ for structurally refined monoclinic and triclinic K-rich alkali feldspars, respectively, plotted against (a) the b cell dimension, (b) $2\theta(060)$, (c) the c^* reciprocal cell dimension, and (d) $2\theta(\bar{2}04)$. Data are from Table 2 and references therein; 2θ values for Cu$K\alpha_1$ radiation were calculated from the lattice parameters of these crystals. The structures of metrically monoclinic samples P2A, P2B, and CA1A were refined in triclinic space group $C\bar{1}$ by Dal Negro et al. (1978, 1980) and thus are presumed to be topochemically triclinic. We used their data in calculating *both* regression lines in each diagram. The Spencer U (SpU) crystal was omitted in the b vs. $(t_1o + t_1m)$ plot because of poor fit.

revised and contoured a vs. $b \cdot c$ plot and a new d_{201} vs. $d_{060} \cdot d_{204}$ plot are presented with formulas to give quantitative estimates of strain.

Determining compositions of alkali feldspars

In our diagrams for determining (Al,Si) distributions of alkali feldspars, compositions often can be approximated with reference to the limiting exchange series whose plotted n_{Or} values are designated at either 0.05 or 0.10 mole fraction intervals. However, to determine Or contents more reliably, one can use the observed volume, V, of the unit cell in one of the three cubic equations listed in Kroll et al. (1986, Table 9, p. 11). These are based on a larger data set and thus are slightly different than those given by Kroll and Ribbe (1983, Eqs. 8a, 8b, 8c). [Note also that there were errors in the latter's Equation 8c (p. 74) in which $-5.96146 \times 10^{-2}V^2$ and $2.91994 \times 10^{-5}V^3$ should have read $-5.96146 \times 10^{-3}V^2$ and $2.91994 \times 10^{-6}V^3$, respectively.] Based on five different alkali-exchange series, Hovis (1986, p. 880) also derived three cubic equations for determining compositions from volume for "disordered feldspars," "relatively ordered topochemically monoclinic feldspars," and for [ordered] "topochemically triclinic" feldspars.

Equations and diagrams for determining structural state

General form of the equations

The determinative equations for both monoclinic and triclinic alkali feldspars are of the form

$$y = A + Bx + C(t_1o \pm t_1m) + DX(t_1o \pm t_1m), \qquad (2)$$

where x and y may be c^* and b, c and b, or $2\theta(\bar{2}04)$ and $2\theta(060)$, respectively. Note that for monoclinic alkali feldspars, $(t_1o + t_1m) = 2t_1$.

This type of equation was introduced by Luth (1974) in an earlier analysis of the variation of b-c and α^*-γ^* with structural state. Use of this equation does assume that the contours of constant $(t_1o \pm t_1m)$ are straight lines,

$$y = A' + B'x,$$

and that the intercepts and slopes of these lines vary linearly with the value of $(t_1o \pm t_1m)$:

$$A' = A + C(t_1o \pm t_1m),$$
$$B' = B + D(t_1o \pm t_1m).$$

Equation 2 is represented by a fan of straight lines in the **x**-**y** plane. The distance between the lines is constant when measured parallel to the **y** axis at a given x, but when measured parallel to the **x** axis at a given y, it varies nonlinearly with $(t_1o \pm t_1m)$, because

$$\left[\frac{\partial y}{\partial(t_1o \pm t_1m)}\right]_x = C + Dx,$$

$$\left[\frac{\partial x}{\partial(t_1o \pm t_1m)}\right]_y = \frac{-C[B + D(t_1o \pm t_1m)] - D[y - A - C(t_1o \pm t_1m)]}{[B + D(t_1o \pm t_1m)]^2}.$$

Blasi (1982) pointed out that in proportionally dividing a quadrilateral with no parallel sides (such as those in Fig. 2) into a series of straight contour lines representing degrees of constant structural state Δ, where $\Delta \equiv (t_1o \pm t_1m)$, the equations of the lines have the general form

$$A\Delta^2 + B\Delta + C = 0,$$

where A, B, and C are functions of the coordinates of the corners and the limiting values of Δ. He found significant systematic differences [up to 0.009 in $(t_1o + t_1m)$ and 0.026 in $(t_1o - t_1m)$] in the positions of the Δ contours determined by his method and the positions determined by the Luth-type Equation 2 for the b-c and α^*-γ^* diagrams in use at the time. We have not adopted Blasi's rigorous method of calculating Δ from lattice parameters (for which he has written a Fortran IV program), because we will show that, in contrast to previous diagrams, departure of the contours on our new diagrams from what we call "proportional contouring" turns out to be negligible.

Rearranging Equation 2, we write it in the form

$$(t_1o \pm t_1m) = \frac{y - A - Bx}{C + Dx}, \qquad (3)$$

and henceforth we minimize the sum of squared residuals in $(t_1o \pm t_1m)$, using the algorithm of Fletcher and Powell (1963). This algorithm is capable of treating equations that are nonlinear in the parameters, like Equation 3, whereas programs for linear regression analysis can only handle equations like Equation 2, minimizing the sum of squared residuals in y, which would be a lattice parameter in our case. Since we want to determine $(t_1o \pm t_1m)$ from lattice parameters, but not vice versa, it is obviously more advisable to use Equation 3 rather than 2, as was done previously. The Fletcher-Powell algorithm was programmed to handle Equation 3 by D. Stöckelmann, Münster.

When calculated from errors of measurement in x and y, the standard error of estimate, σ, is given from the propagation-of-error law by

$$\sigma^2(t_1o \pm t_1m) = (C + Dx)^{-2}\sigma^2(y) + \left[\frac{-B(C + Dx) - D(y - A - Bx)}{(C + Dx)^2}\right]^2 \sigma^2(x). \qquad (4)$$

New determinative methods for Al in the two T_1 sites

Even though it has long been known that plots of the lattice parameters b vs. c are not strictly linear for any Na-K exchange series in which (Al,Si) distribution does not vary, Wright and Stewart (1968), Stewart and Ribbe (1969), and Stewart and Wright (1974) for convenience and as a "reasonable first approximation" assumed that they were. Luth (1974) first highlighted the problem of nonlinearity in b-c and b^*-c^* plots, which is particularly evident in the K-rich end of alkali-exchange paths where most natural samples occur. This point was recently stressed by Hovis (1984, 1986).

In an attempt to linearize alkali-exchange paths, Hovis (1986) devised methods to "correct" the c cell dimension for composition effects. The c_K parameter thus calculated for any specimen is the pure K equivalent, and there is a high correlation between the parameter

$$Z \equiv (t_1o + t_1m) - (t_2o + t_2m) \equiv 2\Sigma t_1 - 1$$

TABLE 5. Standard errors of estimate in the Al contents of the two T_1 sites of monoclinic or the T_1O and T_1m sites of triclinic alkali feldspars

	$\sigma(2t_1)$	$\sigma(t_1o + t_1m)$	Assumed σ(lattice parameters)				
*b-c**	≤0.009	≤0.009	$\sigma(b)$	=	0.002 Å; $\sigma(c^*)$	=	0.000 02 Å^{-1}
060-$\bar{2}$04	≤0.02	≤0.02	$\sigma[2\theta(060)]$	=	$\sigma[2\theta(\bar{2}04)]$	=	0.02°
b-c	≤0.014	≤0.016	$\sigma(b)$	=	$\sigma(c)$	=	0.002 Å

Note: Based on assumed standard errors in various parameters used for estimating $2t_1$ and $(t_1o + t_1m)$.

and c_K for alkali feldspars whose structures are known. A linear regression equation for Z (calculated from mean T–O bond lengths using Eq. 1) in terms of c_K ostensibly has a precision of ±0.03, although propagation of error was not taken into account and, unfortunately, no reference points for completely ordered LA or LM were used to constrain Z to go through 1.00 for these end members.

We have taken a different approach to linearizing our determinative methods for Σt_1. The first step was to plot b and c^* (rather than c) vs. $2t_1$ for 21 topochemically monoclinic and vs. $(t_1o + t_1m)$ for 17 topochemically triclinic K-rich alkali feldspars whose structures are known (Tables 2a and 2b). Figure 1 indicates reasonable linearity of these relationships and those involving the more easily measured 2θ values (Cu$K\alpha_1$ radiation) to the 060 and $\bar{2}04$ peaks. Note that some of the scatter results from the fact that cell parameters and 2θ values were not corrected to correspond to 100 mol% Or. The reference points HS and LM are from Table 4; they were not used in calculating the regression lines. Subsequently, least-squares methods were used to calculate equations of the form of Equation 2 for monoclinic and triclinic alkali feldspars, using *b-c**, $2\theta(060)$-$2\theta(\bar{2}04)$, and solving for $2t_1$ and $(t_1o + t_1m)$ separately. Four new determinative plots are in Figure 2; their equations are

$$2t_1 = \frac{b - 24.8095 + 74.9054c^*}{-3.3261 + 19.5102c^*}, \quad (5)$$

$$(t_1o + t_1m) = \frac{b - 21.5398 + 53.8405c^*}{2.1567 - 15.8583c^*}, \quad (6)$$

$$2t_1 = \frac{2\theta(060) + 12.1814 - 1.040\,93[2\theta(\bar{2}04)]}{0.6112 + 0.015\,92[2\theta(\bar{2}04)]}, \quad (7)$$

$$(t_1o + t_1m) = \frac{2\theta(060) + 8.3063 - 0.964\,59[2\theta(\bar{2}04)]}{-6.5616 + 0.157\,24[2\theta(\bar{2}04)]}. \quad (8)$$

For purposes of comparison, the equations for *b-c* plots (not shown) are

$$2t_1 = \frac{b + 5.1479 - 2.564\,37c}{2.7945 - 0.446\,21c}, \quad (9)$$

$$(t_1o + t_1m) = \frac{b - 1.6757 - 1.613\,88c}{-8.9210 + 1.184\,43c}. \quad (10)$$

Equations 5, 7, and 9 for topochemically monoclinic feldspars were derived starting from the equation of a plane

$$2t_1 = A + Bx + Cy, \quad (11)$$

where x and y have the same meaning as in Equation 2. The coefficients A, B, and C were found from a regression analysis of the appropriate data from the 21 monoclinic specimens in Table 2a, plus reference AA. Σt_1 values were then calculated for the K end members of three of Hovis's (1986) alkali-exchange series ("Eifel sanidine," "orthoclase," and "adularia"). Because the structural state is constant across each series, their K and Na end members provide control on the contour distances on the Na side and were thus added to the data set. The Fletcher-Powell algorithm was finally used to find the coefficients of Equations 5, 7, and 9.

In this way, we account for the fact that the contours of Σt_1 are not parallel in the respective plots, as had previously been assumed by Kroll and Ribbe (1983) for lack of evidence to the contrary. Hovis (1986), however, clearly showed that this simplification is no longer justified.

Equations 6, 8, and 10 for topochemically triclinic alkali feldspars were derived by directly employing the Fletcher-Powell algorithm. Input data came from the 17 specimens of Table 2b, plus reference AA, LA, and LM (all singly weighted; reference data are in Table 4). Equation 4 was used to calculate the standard errors of estimate for Σt_1, and the results are given in Table 5.

The diagrams in Figure 2 are linearly and proportionally contoured between the limiting lines at $\Sigma t_1 = 0.55$ and 1.0; therefore, according to the argument of Blasi (1982; discussed above), deviations from linearity are to

TABLE 6. Compilation of Σt_1 values calculated using Equations 5–10 to illustrate the maximum departure from linearity of these equations (see text for discussion)

Equation	Parameters	Na side	K side
5	*b-c** (monoclinic)	0.756	0.757
6	*b-c** (triclinic)	0.745	0.744
7	060-$\bar{2}$04 (monoclinic)	0.750	0.750
8	060-$\bar{2}$04 (triclinic)	0.746	0.747
9	*b-c* (monoclinic)	0.758	0.758
10	*b-c* (triclinic)	0.736	0.737

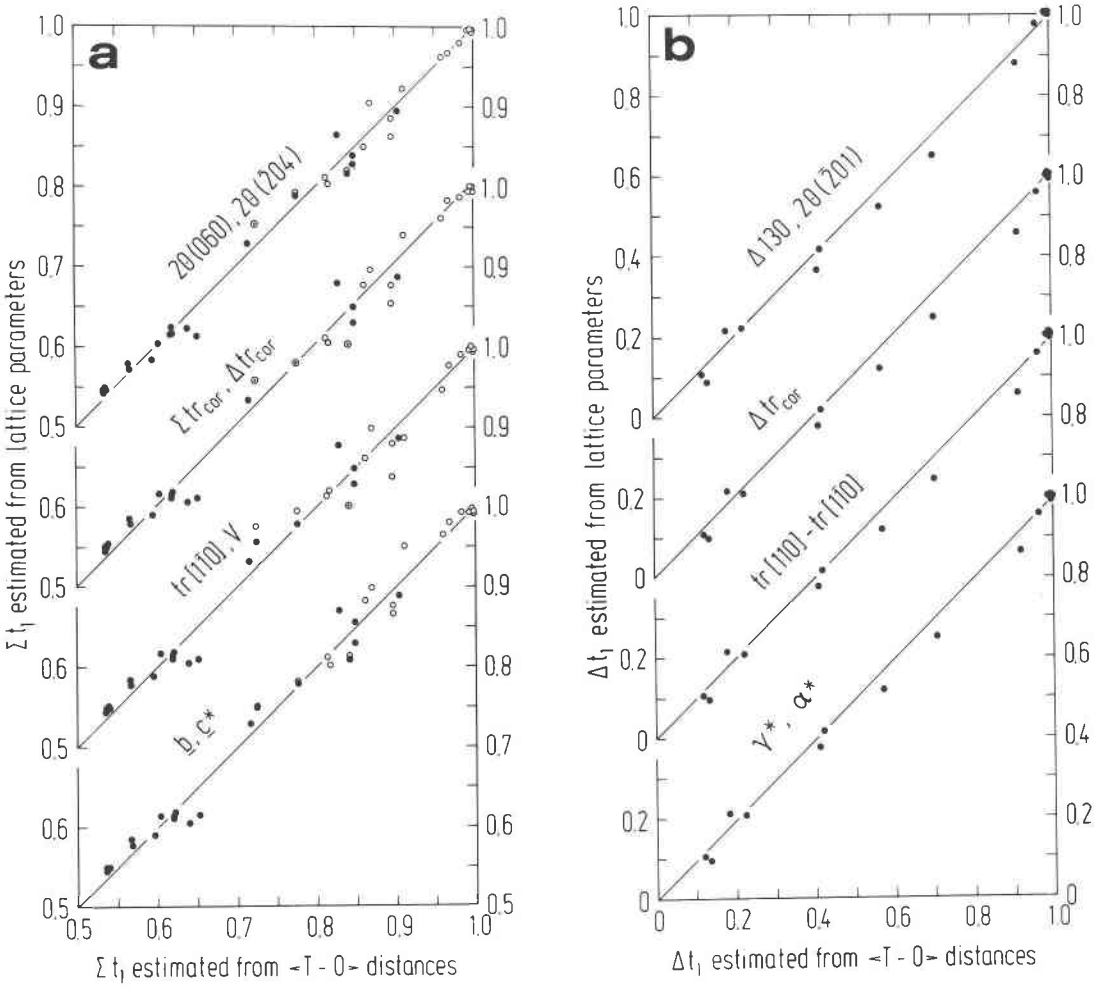

be expected when estimating intermediate values of Σt_1 using Equations 5 to 10. Where proportional contouring would give a result of $\Sigma t_1 = 0.750$, our equations give the values listed in Table 6. These values represent maximum deviations from linearity for the entire range of Σt_1 values that are zero at $\Sigma t_1 = 0.55$ and 1.0. Except for the *b-c* plots and equations, which are no longer recommended for use in structural-state determinations, agreement between Σt_1 values found from proportional contouring and from our equations for the samples in Table 2 is such that neither method is preferred to the other within the limits of estimated standard errors.

The values of $2t_1$ and $(t_1o + t_1m)$ were calculated from Equations 5–10 for individual structures used in the regression analyses. They are plotted versus the values of Σt_1 estimated from ⟨T–O⟩ bond lengths in Figure 3a; all data are in Table 2.

The LA–LM and AA–HS alkali-exchange series of Kroll et al. (1986) and three of Hovis's (1986) series are plotted in Figure 2. Clearly the *b-c** plots give much more nearly linear representations of the series than did the earlier *b-c* and *b**-*c** plots (Luth, 1974, Figs. 9, 10, 14, 15; Kroll and Ribbe, 1983, Fig. 4; Hovis, 1986, Figs. 9 and 10). Departure of these from linearity is relatively small, amounting to less than 0.02 in Σt_1, regardless of composition.

We calculated Σt_1 [$= (Z + 1)/2$] for each specimen in the five alkali-exchange series of Hovis (1986; data in his Table 6), first using our Equations 5 and 6 and then using his Equations 8, 9, 10, and 15. We plotted these values versus composition in Figure 3c. In the four series that have $t_1o = t_1m$ and $t_2o = t_2m$, results are in reasonable agreement, with a somewhat smaller amount of scatter of individual values about the respective mean Σt_1 values when derived from our equations. Differences in mean values of Σt_1 amount to -0.007 to $+0.014$ for those calculated by Hovis's equations. For Hovis's "microcline" series, however, the deviation is large. Use of his equations produces Σt_1 values ranging from 0.940 to 0.983 (mean 0.952), even though the parent material of his "microcline" series is Amelia, Virginia, low albite, which was shown by Smith et al. (1986) to be fully ordered. In contrast, our equations give $\Sigma t_1 = 0.974$ to 1.018 (mean 0.999).

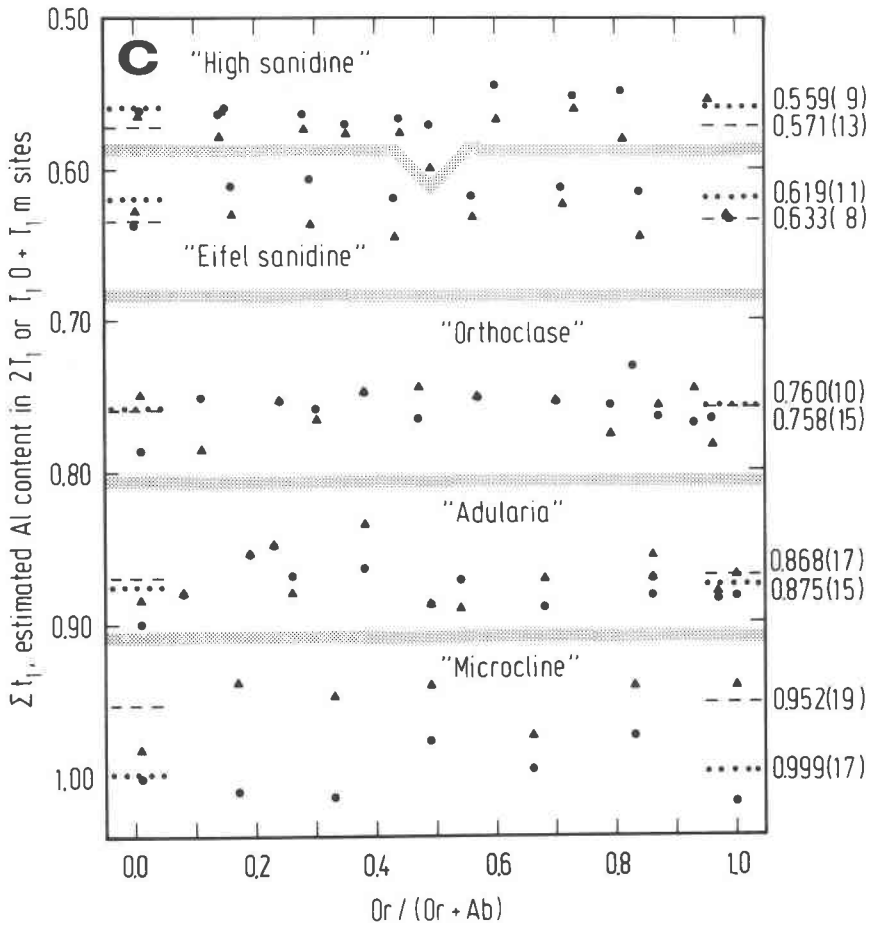

←

Fig. 3a. Plots of Σt_1 determined for monoclinic (dots) and triclinic (circles) alkali feldspars from observed bond lengths (Eq. 1) vs. values calculated using Equations 7 and 8 (top curve), 24 (second curve), 17 and 19 (third curve), and 5 and 6 (bottom curve); data in Table 2.

←

Fig. 3b. Plots of Δt_1 determined for metrically triclinic feldspars from observed bond lengths (Eq. 1) vs. values calculated using Equations 14, 23, 19, and 12, respectively, for the curves from top to bottom; data in Tables 2 and 3.

→

Fig. 3c. Plots of Σt_1 vs. n_{Or} calculated for the five alkali-exchange series of Hovis (1986, Table 6) using our Equations 5 and 6 (dots) and Hovis's Equations 8–10 and 15 (triangles). For each series, horizontal lines connecting the triple dots and the double dashes would represent average Σt_1 values from our equations and those of Hovis, respectively.

Table 2 provides further comparison between our methods and those of Hovis. It is seen that the sum of the differences between Σt_1 values calculated from ⟨T–O⟩ distances and lattice parameters, respectively, is much larger for Hovis's c_K-Z method than for our methods. In case of the triclinic feldspars, this may be attributed to the fact that the Z values were not constrained to 1.0 for low microcline; in case of the monoclinic feldspars, the reason may be more fundamental. Hovis's method is a one-parameter method, and when the c cell edge is affected by strain or by chemical impurities (as observed in the Eifel sanidines), then c_K and Z values are necessarily in error. In contrast, in a two-parameter method, both parameters, e.g., b and c^*, are shifted in the same sense. Thus, a point on a plot like Figure 2 would ideally move along a contour line of constant Σt_1. This compensating effect favors a two-parameter over a one-parameter method.

In summary, the b-c^* method is preferred over the b-c method for determining the total Al content of the T_1 sites in homogeneous alkali feldspars, because (1) data points for all structural states follow nearly linear contours and (2) departure of the equations from proportional contouring is negligible, i.e., $<1\sigma$. It is also preferred over the c_K-Z method, which is a one-parameter method and appears to require some modification. Other determinative methods for Σt_1 involving the translations along the [110] and [1$\bar{1}$0] zones will be discussed separately below.

Determinative methods for ($t_1o - t_1m$)

In fitting the data for determining $\Delta t_1 \equiv (t_1o - t_1m)$ from the reciprocal lattice angles α^* and γ^*, it was necessary to fix *all* end-member values (Table 4); least-squares analysis was not used. The resulting equation for the familiar α^*-γ^* plot, introduced by MacKenzie and Smith (1955) and contoured for Δt_1 by Stewart and Ribbe (1969), is

$$\Delta t_1 = (t_1o - t_1m) = \frac{\gamma^* - 44.778 - 0.50246\alpha^*}{6.646 - 0.05061\alpha^*}. \quad (12)$$

Note that $\alpha^* = \gamma^* = 90°$ and $\Delta t_1 = 0.0$ for all monoclinic feldspars, including all those with $n_{Or} > 0.34$ in the high

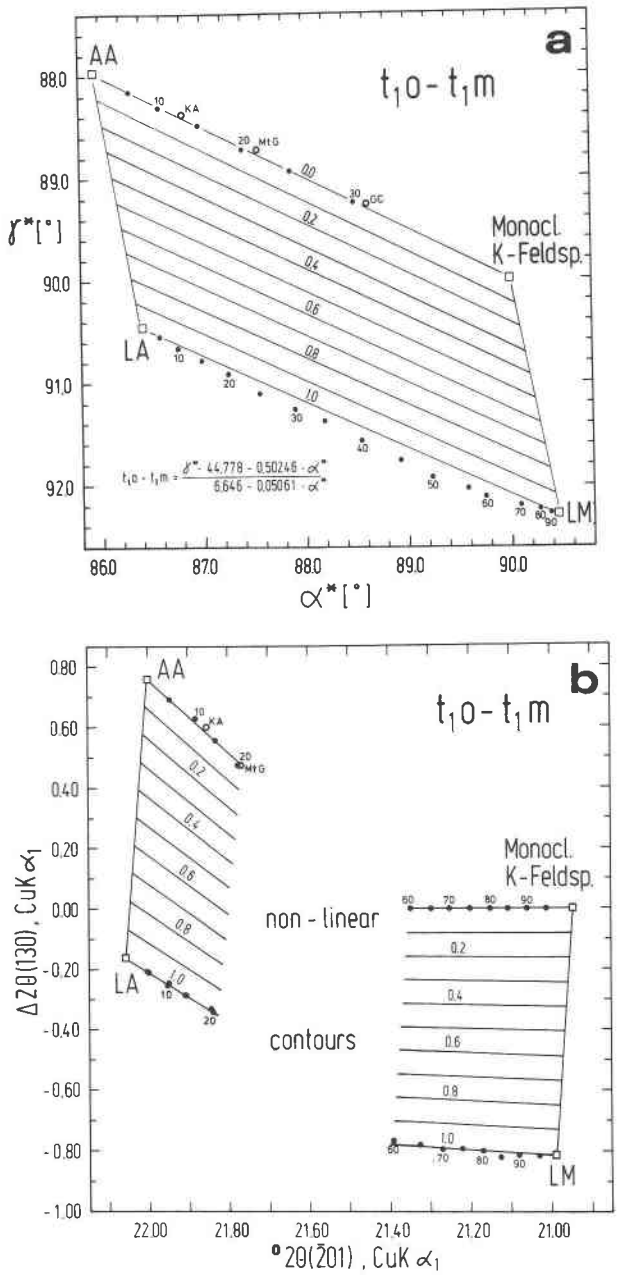

Fig. 4. (a) Plot of the reciprocal lattice angles α^* vs. γ^* based on end-member values (squares) from Table 4 and contoured for $\Delta t_1 = (t_1o - t_1m)$. Dots are data from the LA–LM and AA–HS alkali-exchange series of Kroll et al. (1986); circles are from data (at room temperature) of Harlow (1982) for three natural anorthoclases (K-analbites), all of which inverted to monoclinic symmetry at higher temperatures. (b) Plot of $\Delta 2\theta(130) \equiv [2\theta(130) - 2\theta(1\bar{3}0)]$ vs. $2\theta(\bar{2}01)$, in degrees, for Cu$K\alpha_1$-radiation. Data points as in (a). The graph is not useful for compositions between Or_{20} and Or_{60}.

series, and that the AA–HS exchange series is almost perfectly linear on the α^* vs. γ^* plots (Fig. 4a). However, the LA–LM exchange series of Kroll et al. (1986) does not follow a linear path, with departures of up to 0.09 in Δt_1 at $n_{Or} = 0.5$. Three specimens in the "microcline" series of Hovis (1986) lie closer to the straight line joining LA–LM, but in the range $0.60 < n_{Or} < 1.00$, Hovis's specimens are precisely in register with those of Kroll et al., as is his low albite.

Plots of α vs. γ, α^* vs. γ and α vs. γ^* were made in an attempt to improve the linearity of the LA–LM exchange path, with no success. Fortunately, serious departure from linearity lies outside of the composition range observed in nature for homogeneous feldspars. Other than LA–LM, no complete exchange series of triclinic alkali feldspars is known, although Δt_1 values predicted from α^*–γ^* for Spencer U intermediate microcline and its K- and Na-exchanged equivalents (Wright and Stewart, 1968, Table 2) agree within ± 0.02 of 0.31.

There are two ways to employ Equation 2 and a related equation of type 3 in calculating determinative equations for Δt_1:

$$\gamma^* = A + B\alpha^* + C\Delta t_1 + D\Delta t_1\alpha^*,$$

or

$$\alpha^* = A' + B'\gamma^* + C'\Delta t_1 + D'\Delta t_1\gamma^*.$$

If the former equation is used, as by Luth (1974, p. 277) and Kroll and Ribbe (1983, p. 80), departures from proportional contouring reach values of -0.029 (Blasi, 1982). But if the latter equation is used, the maximum deviation is 0.002 across the entire composition range at $\Delta t_1 = 0.5$, decreasing to zero at $\Delta t_1 = 1.0$ and 0.0, and thus is totally negligible.

The α^*-γ^* method for determining Δt_1 is relatively tedious when used with powdered feldspar samples because the entire diffraction pattern must be measured and indexed and the lattice parameters refined by least-squares methods. However, if 0.3–0.5-mm single crystals are available, the precession technique (Ribbe, 1983, p. 32), readily provides X-ray photographs from which α^* and γ^* may be measured (e.g., see study of Su et al., 1986b, of the LA–HA series).

For unstrained triclinic alkali feldspars it is also possible to use a simplified X-ray powder method to determine $(t_1o - t_1m)$. Figure 4b combines $\Delta 2\theta(130) \equiv 2\theta(130) - 2\theta(1\bar{3}0)$, a γ^*-sensitive parameter, with the 2θ value of $\bar{2}01$, a composition-sensitive peak. The units for both the abscissa and the ordinate are degrees 2θ measured from a diffraction pattern taken with Cu$K\alpha_1$ radiation. Of course, this method is most difficult to use when the 130 and $1\bar{3}0$ peaks are closely overlapped, as they are near $\gamma^* = 90°$.

To obtain the following equations, intercepts and slopes were used for the four lines in Figure 4b, which are drawn through data from Kroll et al. (1986). For the Na-rich side,

$$\Delta t_1 = (t_1o - t_1m) = \frac{\Delta 2\theta(130) + 25.606 - 1.1985[2\theta(\bar{2}01)]}{7.0791 - 0.36583[2\theta(\bar{2}01)]},$$

and for the K-rich side,

$$\Delta t_1 = (t_1o - t_1m) = \frac{\Delta 2\theta(130)}{-2.700 + 0.089\,86[2\theta(\bar{2}01)]}. \quad (14)$$

If standard errors of estimate in $\Delta 2\theta(130)$ and $2\theta(\bar{2}01)$ are $\pm 0.02°$, $\sigma \cong 0.03$ in Δt_1, according to Equation 4. Systematic departures from proportional contouring are negligible. Values of $(t_1o - t_1m)$ were determined from Equations 12 and 14 for metrically triclinic K-rich alkali feldspars. They are listed in Table 3 and plotted on Figure 3b in which they are compared with Δt_1 calculated from bond lengths (Eq. 1). The latter suggests that there may be some nonlinearity that is unaccounted for by our models, but agreement is within $\Delta t_1 = \pm 0.02$ for 9 of 14 specimens. Because our methods are based on lattice parameters, they cannot be used to calculate Δt_1 for topochemically triclinic feldspars that are metrically monoclinic (e.g., specimens P2A, P2B, CA1A).

The [110] methods for determining (Al,Si) distribution

Kroll (1971, 1973, 1980) investigated other parameters that are sensitive to (Al,Si) order-disorder, namely the translation distances in the [110] and [1$\bar{1}$0] directions, tr[110] and tr[1$\bar{1}$0], which may be calculated using equations in Table 4. Because for all feldspars

$$t_2o = t_2m = [1 - (t_1o + t_1m)]/2 = [1 - \Sigma t_1]/2,$$

the major effect on lattice parameters of (Al,Si) ordering or disordering can be traced to the Al content of T_1O and T_1m, expressed in terms of Σt_1 and Δt_1. This is particularly true of the [110] and [1$\bar{1}$0] directions: the sequence of tetrahedral sites along the former is $T_1O \rightarrow T_2O \rightarrow T_2m$ and along the latter $T_1m \rightarrow T_2O \rightarrow T_2m$ (see Fig. 1 in Kroll, 1973, or Fig. 8, Kroll and Ribbe, 1983). Thus it becomes obvious in topochemically monoclinic feldspars, for which $t_1o = t_1m$ and $t_2o = t_2m$, that the [110] and [1$\bar{1}$0] paths through the structure encounter equal "amounts" of Al. But if the structure becomes fully ordered ($t_1o = 1.0$), all the Al is concentrated along [110] and none of it along [1$\bar{1}$0]. Therefore, tr[110] and tr[1$\bar{1}$0] vary in opposite directions with increasing order, particularly as the T_1m site "empties" Al into T_1O. The Al content of T_2 sites has no *differential* effect on the two translation distances.

The variation of tr[110] and tr[1$\bar{1}$0] in K-feldspars is shown in Figure 5 (see Kroll and Ribbe, 1983, p. 88, for a discussion). Both parameters were corrected to correspond to $n_{Or} = 1$, following the procedure described below.

To make Figure 5 useful for estimating t_1o in alkali feldspars of any composition, tr[1$\bar{1}$0] has been plotted versus cell volume V and contoured for t_1 and t_1o, respectively. This was done by Kroll and Ribbe (1983, Fig. 10, p. 90). Although the figure is not reproduced, new equations calculated from the increased data base are discussed here. The Na- and K-rich sides of their Figure 10 had to be considered as separate entities because a distinct change in slope of tr[1$\bar{1}$0] vs. V lines occurs between Or_{30} and Or_{40}.

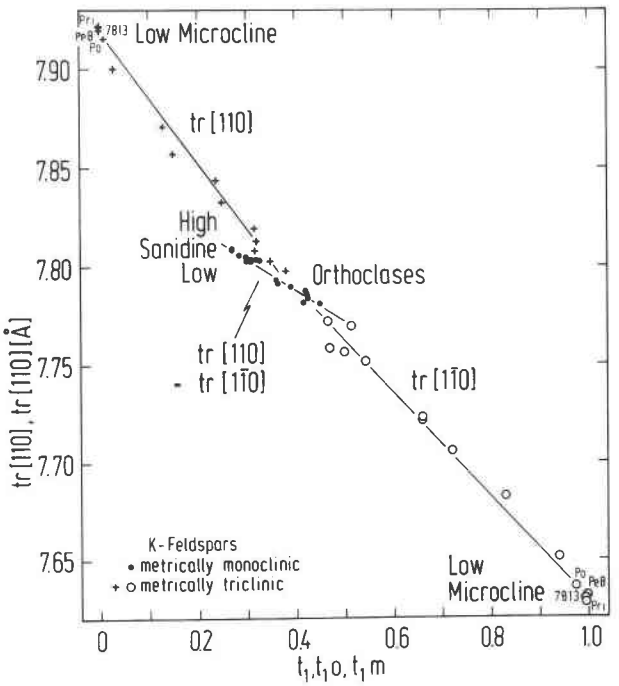

Fig. 5. Variation of tr[110] (= tr[1$\bar{1}$0]) for metrically monoclinic K-rich feldspars (dots) with t_1 and Al content of the T_1 site (central line). Variation for metrically triclinic K-feldspars of tr[110] with t_1m = Al content of the T_1m site (crosses) and of tr[1$\bar{1}$0] with t_1o = Al content of T_1O site (circles). Values for both tr[110] and tr[1$\bar{1}$0] were corrected using Equations 21 and 22 so that all compositions correspond to $n_{Or} = 1$. Four low microclines are labeled; see Table 2 for references.

For the topochemically monoclinic K-rich feldspars ($V \geq 692$ Å^3), a regression equation was calculated using the 21 structures of Table 2a plus a fixed point chosen at $V = 692$ Å^3 on the Na-sanidine line in their Figure 10:

$$t_1 = 36.030 - 6.5690\text{tr}[1\bar{1}0] + 0.021\,478V. \quad (15)$$

The equivalent equation for topochemically monoclinic Na-rich feldspars ($V < 692$ Å^3) was calculated using as fixed points reference AA plus a point on the K-analbite line and assuming that the change of tr[1$\bar{1}$0] with t_1 is identical on the Na- and K-rich sides:

$$t_1o = t_1m = 37.165 - 6.5690\text{tr}[1\bar{1}0] + 0.019\,898V. \quad (16)$$

The error-propagaton law (Eq. 4) gives $\sigma(t_1) = \sigma(t_1o) = 0.014$, assuming $\sigma(\text{tr}[1\bar{1}0]) = 0.002$ Å and $\sigma(V) = 0.3$ Å^3 for both Equation 15 and 16.

Contouring of the topochemically triclinic alkali feldspars follows a similar procedure. For the K-rich side, the input to the Fletcher-Powell program consisted of data for the 17 structures of Table 2b, including reference LM and two fixed points chosen at $V = 692$ Å^3 on the LA–

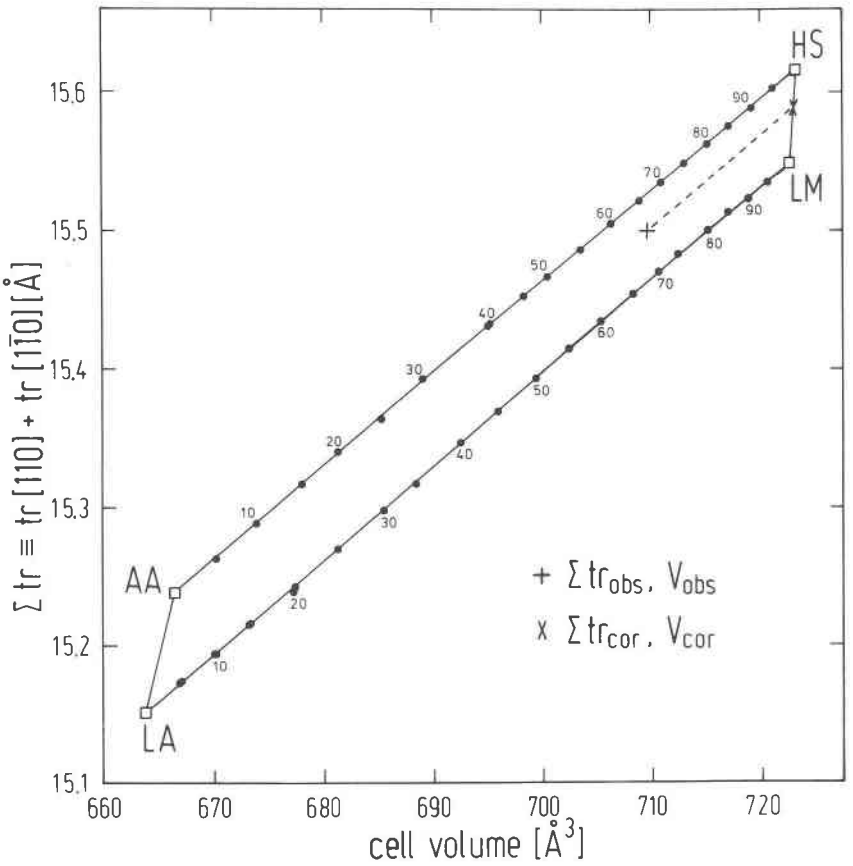

Fig. 6. The parameter $\Sigma tr \equiv tr[110] + tr[1\bar{1}0]$ vs. V, unit-cell volume, for alkali feldspar series. Data points as in Figure 4. + ----- × represents an extrapolation to correct Σtr for composition, as explained in the text.

LM line and on the $t_1 = 0.4$ contour, respectively (Eq. 15). The equation is

$$t_1o = \frac{tr[1\bar{1}0] - 5.6954 - 3.0406 \times 10^{-3}V}{-0.67815 + 5.7439 \times 10^{-4}V}. \quad (17)$$

For the Na-rich side ($V < 692$ Å), the same two fixed points were used with reference AA and LA to arrive at

$$t_1o = \frac{tr[1\bar{1}0] - 5.3327 - 3.5620 \times 10^{-3}V}{0.18238 - 6.6729 \times 10^{-4}V}. \quad (18)$$

The error-propagation law gives $\sigma(t_1o) = 0.008$ assuming $\sigma(tr[1\bar{1}0]) = 0.002$ Å and $\sigma(V) = 0.3$ Å^3 for both Equations 17 and 18.

Figure 5 suggests that the difference in length $\Delta tr \equiv tr[110] - tr[1\bar{1}0]$ is very sensitive to Δt_1. Values of Δtr vs. V were plotted and contoured for Δt_1 by Kroll and Ribbe (1983, p. 92) in their Figure 11. Similar to their Figure 10, the K- and Na-rich sides were treated separately. The equation for K-rich feldspars ($V \geq 692$ Å^3) was derived from reference HS and LM and two fixed points taken at the intersection of the AA–HS and LA–LM straight line segments at $V = 692$ Å^3:

$$\Delta t_1 = (t_1o - t_1m) = \frac{\Delta tr}{0.6457 - 0.4902 \times 10^{-3}V}. \quad (19)$$

For the Na-rich side ($V < 692$ Å^3), from the same two fixed points plus reference AA and LA, we find

$$\Delta t_1 = (t_1o - t_1m) = \frac{\Delta tr + 0.8393 - 0.1213 \times 10^{-2}V}{0.4579 - 0.2196 \times 10^{-3}V}. \quad (20)$$

Assuming $\sigma(\Delta tr) = 0.003$ Å and $\sigma(V) = 0.3$ Å^3, the error-propagation law gives $\sigma(\Delta t_1) = 0.010$ for both Equations 19 and 20.

The variation of $tr[110]$ and $tr[1\bar{1}0]$ with t_1o and t_1m was demonstrated in Figure 5 using values that were corrected to correspond to $n_{Or} = 1$. The correction procedure is most easily formulated in terms of the difference and the sum of the two translation distances: $\Delta tr \equiv tr[110] - tr[1\bar{1}0]$ (Kroll and Ribbe, 1983, Fig. 11) and $\Sigma tr \equiv tr[110] + tr[1\bar{1}0]$ (Fig. 6), and when applied to these two quantities, it provides another useful diagram (Fig. 7). The procedure works as follows: Assume a data point ($\Delta tr_{obs}, V_{obs}$)

to plot within the K-rich region of Kroll and Ribbe's Figure 11. When projecting this point along the contour line on which it plots to the intersection with the HS–LM line, we get a new, corrected Δtr_{cor} value corresponding to $n_{Or} = 1$. The equation describing this procedure is

$$\Delta tr_{cor} = p + \left(\frac{i - p}{q - s}\right) q, \tag{21}$$

where $p = 334.822$, $b = -0.4902 \times 10^{-3}$, $q = -0.4629$, $i = a\Delta tr_{obs}/(a + bV_{obs})$, $a = 0.6457$, $s = b\Delta tr_{obs}/(a + bV_{obs})$.

In a similar way we proceed in a plot of Σtr vs. V to get a corrected Σtr_{cor} value. On Figure 6, for instance, consider the point "+" = $(\Sigma tr_{obs}, V_{obs})$. We find the corrected "×" = $(\Sigma tr_{cor}, V_{cor})$ at the intersection of the dashed line with the HS–LM line. Because, unlike Figure 11 of Kroll and Ribbe (1983), the AA-HS and LA–LM lines are parallel to each other in the K-rich region, the correction equation becomes

$$\Sigma tr_{cor} = p + \left(\frac{i - p}{q - s}\right) q, \tag{22}$$

where $p = -60.543$, $q = 0.1053$, $s = 0.6553 \times 10^{-2}$, and $i = \Sigma tr_{obs} - sV_{obs}$.

After applying this correction procedure, it is now feasible to plot Figure 7, which is a graph of the parameters Δtr_{cor} vs. Σtr_{cor} for K-rich feldspars (corrected to $n_{Or} = 1.00$). It has been contoured for Σt_1 and Δt_1. The latter values were calculated from HS and LM end-member data only (Table 4); the equation is simply

$$\Delta t_1 = (t_1o - t_1m) = 3.4341\Delta tr_{cor}. \tag{23}$$

The contours for Σt_1 were calculated using all monoclinic and triclinic feldspars from Table 2, plus reference LM (Table 4; weighted × 10); the result is

$$\Sigma t_1 = (t_1o + t_1m) = 96.996 - 6.1762\Sigma tr_{cor} + 0.1258\Delta tr_{cor}. \tag{24}$$

The propagation-of-error law gives $\sigma(\Delta t_1) = 0.01$ and $\sigma(\Sigma t_1) = 0.02$, assuming $\sigma(\Sigma tr_{cor}) = \sigma(\Delta tr_{cor}) = 0.003$ Å.

Figure 7 illustrates the position of natural intermediate microclines between the extremes of the two- and one-step ordering processes (Ribbe, 1983, p. 24–29, and Kroll and Ribbe, 1983, p. 96–99) and at the same time provides an estimate of T site occupancies, determined from cell parameters.

Evaluation

Pairs of diagrams like b-c^* and α^*-γ^* (Figs. 2a and 2b) or tr[1$\bar{1}$0]-V and Δtr-V (Kroll and Ribbe, 1983, Figs. 10 and 11), or the Σtr-Δtr plot (Fig. 7) provide complete estimation of the (Al,Si) distribution among the nonequivalent T sites of alkali feldspars. Agreement of the various methods is good, as may be seen from a comparison of the results displayed in Figures 3a and 3b and Tables 2 and 3. Differences among the methods are, for example, the following:

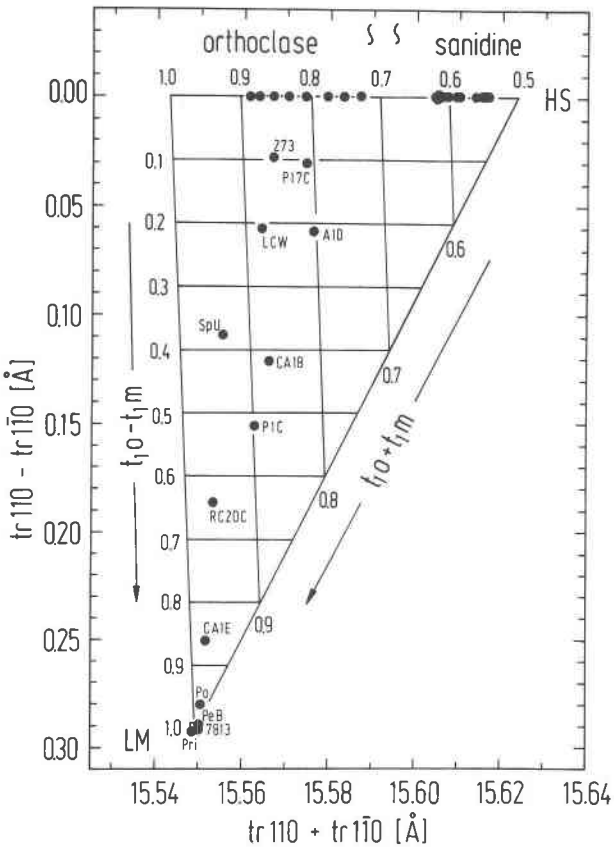

Fig. 7. Plot of $\Delta tr \equiv tr[110] - tr[1\bar{1}0]$ vs. $\Sigma tr \equiv tr[110] + tr[1\bar{1}0]$, both of which have been corrected to $n_{Or} = 1$ using Equations 21 and 22. Contours for $\Sigma t_1 \equiv (t_1o + t_1m)$ and $\Delta t_1 \equiv (t_1o - t_1m)$ are given and permit graphical evaluation of structural state of the natural and heated natural specimens whose lattice parameters may be found in references given in Table 2. The diagonal line joining LM and HS represents the hypothetical "one-step" ordering path, and the horizontal and vertical boundaries of the triangle represent the extreme ideal "two-step" ordering path.

In contrast to the b-c^* and α^*–γ^* method, departure from proportional contouring need not be considered with tr[110],tr[1$\bar{1}$0] diagrams because the AA–LA and HS–LM lines are virtually parallel to the y axis such that the distance between the contours is constant along these lines (also see section on the "General form of the equations").

When compared to the α^*-γ^* diagram, it is seen that in the Δtr-V plot, no systematic deviation from linearity occurs in the LA–LM series. However, complications arise with K-analbites, which plot slightly below the limiting $\Delta t_1 = 0$ line, when produced by Na exchange from orthoclase. In all other cases, including natural samples, they plot on or above that line, as they should.

In diagrams of tr[110] vs. tr[1$\bar{1}$0], contours of constant Or content are roughly equidistant because V is plotted on the abscissa, whereas in b-c^* and α^*-γ^* diagrams, it is almost impossible to resolve K-rich compositions, all being crowded near the HS–LM side.

The tr[1$\bar{1}$0]-V diagram provides high resolution for t_1o in topochemically triclinic feldspars, but resolution is poor for t_1 or t_1o in topochemically monoclinic ones, only about 70% of that available using the b-c* diagram.

In summary, each determinative method has its own inherent advantages and disadvantages, and the reader may choose among them, depending on the specific purpose.

Strain index for alkali feldspar intergrowths

To this point, our discussion has presumed that the feldspars evaluated by the various determinative methods are either homogeneous single phases or phases that are essentially unaffected by strain. In alkali feldspars, however, strain may result from structural coherency between intergrown K- and Na-rich phases that have exsolved from what was once a single, homogeneous feldspar crystal at some higher temperature. Continuity of the aluminosilicate framework is preserved as nearly as possible across the interface between the phases as K and Na segregate, but because of their difference in size, considerable strain may be evident in both phases. This is manifested in adjustments of bond lengths and bond angles that affect cell dimensions, especially a, up to 5%. See discussions by Brown and Willaime (1974), Tullis (1975), Yund and Tullis (1983a, 1983b), and Griffen and Johnson (1984).

Stewart and Wright (1974, p. 362f) suggested a method of estimating strain by using a b-c plot that is contoured for a as determined from homogeneous alkali feldspars. The observed b and c parameters of the uncharacterized feldspar are plotted on this diagram, and a is estimated from the contours. A parameter, Δa, is calculated by subtracting the estimated value of a from the observed value. Stewart (1975) has warned that "the effects of certain components . . . (B, Fe, NH_4^+, and H_3O^+?) may be confused with the effects of coherence."

In the interest of characterizing the degree of strain of K- and Na-rich phases from crypto- or microperthitic intergrowths, we have plotted a vs. $b \cdot c$ in Figure 8a and d_{201} vs. $d_{060} \cdot d_{204}$ in Figure 8b, in a manner discussed by Bernotat (1982). In each plot, an approximate contour has been fitted to the combined LA–LM and AA-HS alkali exchange data of Kroll et al. (1986). This is the approximate locus of parameters for unstrained alkali feldspars.

We have contoured the "strain diagram" (Fig. 8a) by defining 100% strain on a HS coherently intergrown with an (unstrained) AA to mean that

$$(b \cdot c)_{\mathrm{HS(strained)}} = (b \cdot c)_{\mathrm{AA(unstrained)}} = 91.49 \text{ Å}^2,$$

such that this strained HS has

$$a \equiv V_{\mathrm{HS}}/(b \cdot c)_{\mathrm{AA}} \sin \beta_{\mathrm{HS}} = 723.3/[12.871 \cdot 7.108 \cdot \sin (116.0°)] = 8.797 \text{ Å}.$$

Likewise, 100% strain on a LA in association with an (unstrained) LM means

$$(b \cdot c)_{\mathrm{LA(strained)}} = (b \cdot c)_{\mathrm{LM(unstrained)}} = 93.62 \text{ Å}^2.$$

such that this strained LA has

$$a \equiv V_{\mathrm{LA}}(b \cdot c)_{\mathrm{LM}} \sin \beta_{\mathrm{LA}} = 663.8/[12.963 \cdot 7.222 \cdot \sin (116.6°)] = 7.930 \text{ Å}.$$

The straight-line segments have equations

$$a = -49.867 + 0.625\,15(b \cdot c)$$

for the K-rich side and

$$a = -5.304 + 0.146\,87(b \cdot c)$$

for the Na-rich side. Combination of these equations with the foregoing reference points for "100% strained" HS and LA produces equations for the strain index (S.I., in %) of the type

$$\text{S.I.} = A + Ba + C(b \cdot c).$$

For the K-rich side,

$$\text{S.I.} = 3391.84 + 67.960a - 42.516(b \cdot c). \quad (25)$$

For the Na-rich side,

$$\text{S.I.} = 1028.00 + 193.883a - 28.472(b \cdot c). \quad (26)$$

Strain indexes were calculated for all the data points on Figure 8a using equations (25) and (26). Then regression analysis was used to find coefficients A, B, and C in the equation

$$\text{S.I.} = A + B[d_{201}] + C[d_{060} \cdot d_{204}],$$

resulting in $A = 3165.74$, $B = 156.080$, and $c = -982.033$ for K-rich compositions and A = 270.37, $B = 474.866$, and $C = -575.721$ for Na-rich compositions and the contours shown on Figure 8b.

For 23 of the K-rich feldspars, agreement between strain indexes estimated by the two methods is within ~1%, although for specimen L29 they differ by nearly 5%. For the six Na-rich feldspars, agreement averages ~2%. Given the simplistic approach to fitting the S.I. = 0% contours, these agreements are reasonable. We recommend the use of Figure 8 in obtaining *relative* strain values whenever crypto- or microperthitic intergrowths are involved. Stewart's (1975) caution regarding the possibility that the effects of other components (B^{3+}, Fe^{3+}, NH_4^+) may mimic strain requires further investigation, but the effects of the common substituents are about S.I. = +1.5% per mole percent anorthite and about −2% per mole percent celsian, based on the positions of their a vs. $(b \cdot \frac{1}{2}c)$ values on these plots.

Summary

The methods for determining (Al,Si) distribution among the nonequivalent tetrahedral sites of alkali feldspars are all model-dependent, including the one used in obtaining the reference points from ⟨T–O⟩ bond lengths in crystal-structure refinements (Eq. 1), against which we have tested all our parameters (Tables 2 and 3, Figs. 3a and 3b). Happily, there is at least an internal consistency among

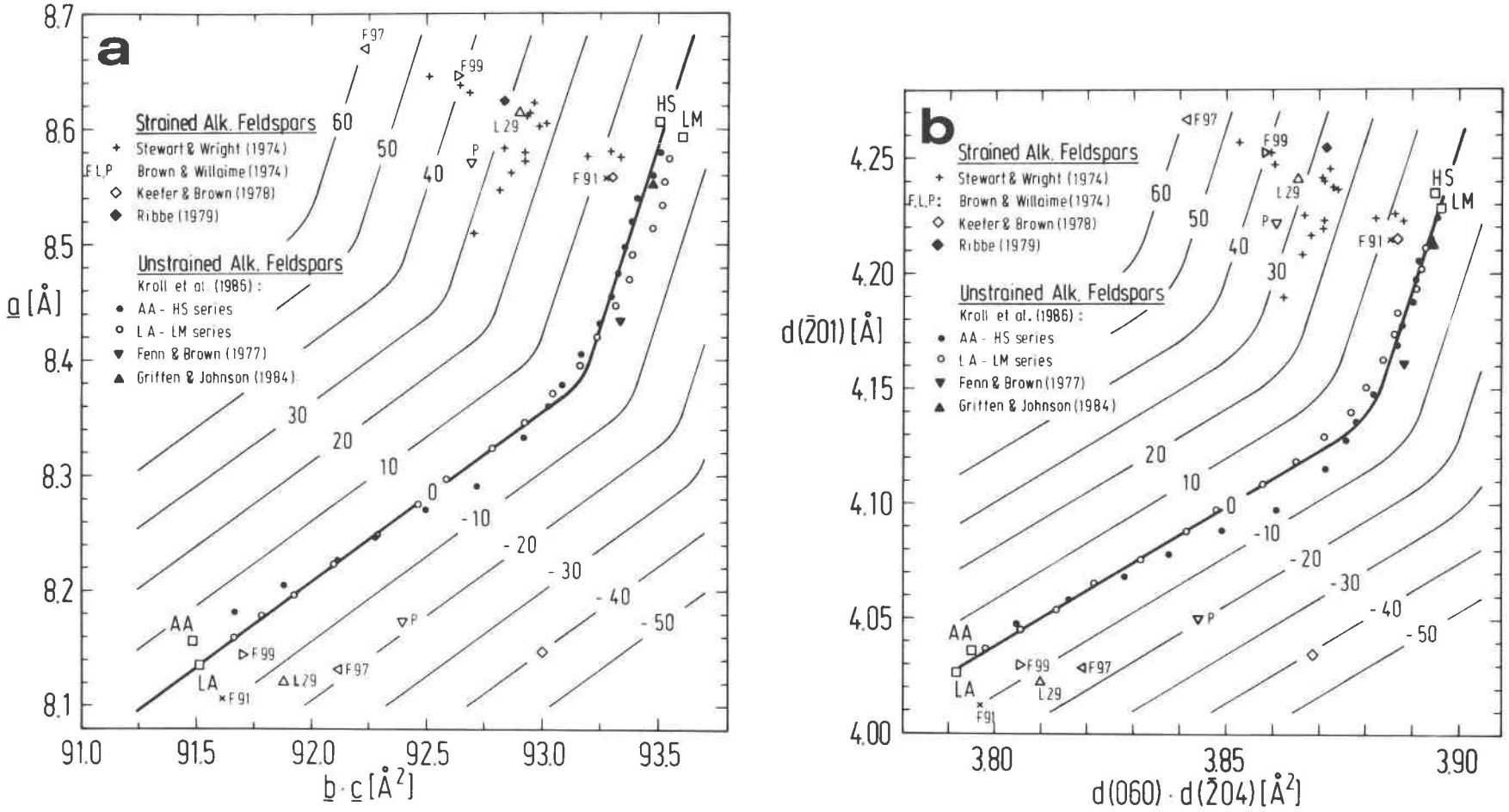

Fig. 8. Plots of lattice-parameter data for unstrained alkali feldspars (heavy line, strain index = 0) and strained phases (K-rich have S.I. > 0, Na-rich have S.I. < 0). (a) The a vs. $b \cdot c$ plot and (b) the d_{201} vs. $d_{060} \cdot d_{204}$ plot; both are contoured for strain index as defined in the text.

them, with $\Sigma t_1 = 2t_1$ or $(t_1o + t_1m)$ estimated to about ± 0.02 and $\Delta t_1 = (t_1o - t_1m)$ to about ± 0.03. Su et al. (1986a) obtained comparable precision in estimating Σt_1 from optic axial angle $2V$ for 109 homogeneous alkali feldspars of known composition; they used the lattice-parameter models in this paper to estimate Σt_1 and thus to calculate their determinative curves.

Acknowledgments

We are grateful to Dr. S. C. Su and Prof. G. L. Hovis for helpful comments on the manuscript, to Mrs. Margie Sentelle for typng, to Mrs. I. Schmiemann for drafting the figures, and to Mrs. G. von Cölln for compiling the tables. Special thanks are due to Dr. D. Stöckelmann, Münster, who programmed the Fletcher-Powell algorithm to treat the nonlinear equations used in this paper. This project received support from National Science Foundation Grant EAR 83-08308 to P.H.R. and F. D. Bloss.

References

Bernotat, W.H. (1982) Ein neues Mass für die Verzerrung der Kristallgitter in entmischten Alkalifeldspäten. Fortschritte der Mineralogie, 60[1], 43–45.

Blasi, A. (1982) Appraisal of the Ferguson method and the linear model using $\Delta(bc)$, $\Delta(\alpha\gamma)$, $\Delta(\alpha^*\gamma^*)$ to estimate tetrahedral Al-contents in alkali feldspars. Mineralogical Magazine, 46, 465–468.

Blasi, A., DePol Blasi, C., and Zanazzi, P.F. (1985). Pellotsalo maximum low microcline: Its structure re-refinement and mineralogical implications. European Union of Geosciences Meeting III, Strasbourg, France April 1–4, 1985, Program with Abstracts, 21.

Brown, W.L., and Willaime, C. (1974) An explanation of exsolution orientations and residual strain in cryptoperthites. In W.S. MacKenzie and J. Zussman, Eds., The feldspars. Manchester University Press, Manchester, p. 440–459.

Dal Negro, A., DePieri, R., Quareni, S., and Taylor, W.H. (1978) The crystal structures of nine K feldspars from the Adamello Massif (northern Italy). Acta Crystallographica, B34, 2699–2707.

Dal Negro, A., DePieri, R., and Quareni, S. (1980) The crystal structures of nine K feldspars from the Adamello Massif (northern Italy): Erratum. Acta Crystallographica, B36, 3211.

DePieri, R. (1979) Cell dimensions, optic axial angle and structural state in triclinic K-feldspars of the Adamello Massif (Northern Italy). Memorie degli Istituti di Geologia e Mineralogia dell' Università di Padova, 32, 17 p.

Fenn, P.M., and Brown, G.E. (1977) Crystal structure of a synthetic, compositionally intermediate, hypersolvus alkali feldspar: Evidence for Na,K site ordering. Zeitschrift für Kristallographie, 145, 124–145.

Fletcher, R., and Powell, M.J.D. (1963) A rapid descent method for minimization. Computer Journal, 6, 163–168.

Gehring, E. (1985) Silizium/Aluminium-Ordnung und Kristallperfektion von Sanidinen. Dissertation, Universität Karlsruhe, West Germany.

Griffen, D.T., and Johnson, B.T. (1984) Strain in triclinic alkali feldspars: A crystal structure study. American Mineralogist, 69, 1072–1077.

Harlow, G.E. (1982) The anorthoclase structures: The effects of temperature and compositions. American Mineralogist, 67, 975–996.

Harlow, G.E., and Brown, G.E., Jr. (1980) Low albite: An X-ray and neutron diffraction study. American Mineralogist, 65, 986–995.

Hovis, G.L. (1984) Characterization of Al-Si distribution in alkali feldspars. Geological Society of America Abstracts with Programs, 16, 544.

——— (1986) Behavior of alkali feldspars: Crystallographic properties and characterization of composition and Al-Si distribution. American Mineralogist, 71, 869–890.

Keefer, K.D., and Brown, G.E. (1978) Crystal structures and compositions of sanidine and high albite in cryptoperthitic intergrowth. American Mineralogist, 63, 1264–1273.

Kroll, H. (1971) Determination of Al,Si distribution in alkali feldspars from X-ray powder data. Neues Jahrbuch für Mineralogie Monatshefte, 91–94.

——— (1973) Estimation of the Al,Si distribution of feldspars from the lattice translations Tr[110] and Tr[1$\bar{1}$0]. I. Alkali feldspars. Contributions to Mineralogy and Petrology, 36, 141–156.

——— (1980) Struktur und Metrik der Feldspäte. Habilitationsschrift, Westfälische Wilhelms-Universität, Münster, West Germany.

Kroll, H., and Ribbe, P.H. (1983) Lattice parameters, composition and Al,Si order in alkali feldspars. Mineralogical Society of America Reviews in Mineralogy, 2, 2nd edition, 57–99.

Kroll, H., Schmiemann, I., and von Cölln, G. (1986) Feldspar solid solutions. American Mineralogist, 71, 1–16.

Luth, W.C. (1974) Analysis of experimental data on alkali feldspars: Unit cell parameters and solvi. In W.S. MacKenzie and J. Zussman, Eds., The feldspars. Manchester University Press, Manchester, p. 249–296.

MacKenzie, W.S., and Smith, J.V. (1955) The alkali feldspars: I. Orthoclase-microperthites. American Mineralogist, 40, 707–732.

Phillips, M.W., and Ribbe, P.H. (1973) The variation of tetrahedral bond lengths in sodic plagioclase feldspars. Contributions to Mineralogy and Petrology, 39, 327–339.

Ribbe, P.H. (1979) The structure of a strained intermediate microcline in cryptoperthitic association with twinned plagioclase. American Mineralogist, 64, 402–408.

——— (1983) Aluminum-silicon order in feldspars; domain textures and diffraction patterns. Mineralogical Society of America Reviews in Mineralogy, 2, 2nd edition, 21–55.

——— (1984) Average structures of alkali and plagioclase feldspars: Systematics and applications. In W.L. Brown, Ed., Feldspars and feldspathoids. NATO AS1 series C, 137, 1–54.

Smith, J.V., Artioli, G., and Kvick, Å. (1986) Low albite $NaAlSi_3O_8$: Neutron diffraction study of crystal structure at 13 K. American Mineralogist, 71, 727–733.

Stewart, D.B. (1975) Lattice parameters, composition and Al/Si order in alkali feldspars. Mineralogical Society of America Short Course Notes, 2, 1st edition, St-23–St-30.

Stewart, D.B., and Ribbe, P.H. (1969) Structural explanation for variations in cell parameters of alkali feldspar with Al/Si ordering. American Journal of Science, 267-A, 444–462.

Stewart, D.B., and Wright, T.L. (1974) Al/Si order and symmetry of natural alkali feldspars, and the relationship of strained cell parameters to bulk composition. Bulletin de la Société française de Minéralogie et de Cristallographie, 97, 356–377.

Strob, W. (1983) Strukturverfeinerung eines Tief-Mikroklins, Zusammenhange zwischen ⟨T–O⟩ Abstanden und Al,Si-Ordnungsgrad und metrische Variation in einer Tief-Albit/Tief-Mikrolin-Mischkristallreihe. Diplomarbeit, Westfälische Wilhelms-Universität, Münster, West Germany.

Su, S.C., Ribbe, P.H., and Bloss, F.D. (1986a) Alkali feldspars: Structural states determined from composition and optic axial angle $2V$. American Mineralogist, 71, 1285–1296.

Su, S.C., Ribbe, P.H., Bloss, F.D., and Goldsmith, J.R. (1986b) Optical properties of single crystals in the order-disorder series low albite–high albite. American Mineralogist, 71, 1384–1392.

Tullis, J. (1975) Elastic strain effects in coherent perthitic feldspars. Contributions to Mineralogy and Petrology, 49, 83–91.

Wright, T.L. (1968) X-ray and optical study of alkali feldspar II. An x-ray method of determining the composition and structural state from measurement of 2θ values for three reflections. American Mineralogist, 53, 88–104.

Wright, T.L., and Stewart, D.B. (1968) X-ray and optical study of alkali feldspar: I. Determination of composition and structural state from refined unit-cell parameters and $2V$. American Mineralogist, 53, 38–87.

Yund, R.A., and Tullis, J. (1983a) Strained cell parameters for coherent lamellae in alkali feldspars and iron-free pyroxenes. Neues Jahrbuch für Mineralogie Monatshefte, 22–34.

——— (1983b) Subsolidus phase relations in the alkali feldspars with emphasis on coherent phases. Mineralogical Society of America Reviews in Mineralogy, 2, 2nd edition, 141–169.

Manuscript received April 2 1986
Manuscript accepted January 26, 1987